

Quantitation of in vivo human folate metabolism¹⁻³

Yumei Lin, Stephen R Dueker, Jennifer R Follett, James G Fadel, Ali Arjomand, Philip D Schneider, Joshua W Miller, Ralph Green, Bruce A Buchholz, John S Vogel, Robert D Phair, and Andrew J Clifford

ABSTRACT

Background: A quantitative understanding of human folate metabolism is needed.

Objective: The objective was to quantify and interpret human folate metabolism as it might occur in vivo.

Design: Adults ($n = 13$) received 0.5 nmol [¹⁴C]pteroylmonoglutamate (100 nCi radioactivity) plus 79.5 nmol pteroylmonoglutamate in water orally. ¹⁴C was measured in plasma, erythrocytes, urine, and feces for ≥ 40 d. Kinetic modeling was used to analyze and interpret the data.

Results: According to the data, the population was healthy and had a mean dietary folate intake of 1046 nmol/d, and the apparent dose absorption of ¹⁴C was 79%. The model predictions showed that only 0.25% of plasma folate was destined for marrow, mean bile folate flux was 5351 nmol/d, and the digestibility of the mix (1046 + 5351 nmol/d) was 92%. About 33% of visceral pteroylmonoglutamate was converted to the polyglutamate form, most of the body folate was visceral (>99%), most of the visceral folate was pteroylpolyglutamate (>98%), total body folate was 225 μ mol, and pteroylpolyglutamate synthesis, recycling, and catabolism were 1985, 1429, and 556 nmol/d, respectively. Mean residence times were 0.525 d as visceral pteroylmonoglutamate, 119 d as visceral pteroylpolyglutamate, 0.0086 d as plasma folate, and 0.1 d as gastrointestinal folate.

Conclusions: Across subjects, folate absorption, bile folate flux, and body folate stores were larger than prior estimates. Marrow folate uptake and pteroylpolyglutamate synthesis, recycling, and catabolism are saturable processes. Visceral pteroylpolyglutamate was an immediate precursor of plasma *p*-aminobenzoylglutamate. The model is a working hypothesis with derived features that are explicitly model-dependent. It successfully quantitated folate metabolism, encouraging further rigorous testing. *Am J Clin Nutr* 2004;80:680-91.

KEY WORDS Folate, metabolism, ¹⁴C, accelerator mass spectrometry, kinetic model

INTRODUCTION

A steady supply of dietary folate is needed to maintain biochemical reactions that include purine and pyrimidine synthesis and the metabolism of homocysteine to methionine. The complex interactions of genetic and dietary factors can cause irregularities in the supply and metabolism of folate and lead to serious health problems.

Although folate has been studied extensively (1-5), the quantitative aspects of folate metabolism in humans are still of considerable interest. Once radiolabeled folate becomes available, key aspects of folate metabolism can be quantified. Prior estimates indicate that $\leq 95\%$ of an oral dose of [³H]pteroylmonoglutamate is absorbed, and that the radiolabel peaks in serum 1-2 h after the dose (6). Furthermore, during the first 12 h after the oral dose, up to 16% of the label is eliminated in the urine. This percentage rises to 41% with an adjuvant 34 000-nmol flushing dose of folate 1 d before (6) but not after (7) the oral dose. Previous findings also indicated that an intravenous dose of [³H]pteroylmonoglutamate promptly disappears from plasma into cells, where it is converted into nondisplaceable forms (8). Another study showed that folate is removed from the blood by the liver and is secreted in human bile at a higher concentration than was present in serum (9). These investigators hypothesized that the excretion of folate in bile might lead to folate depletion in persons with chronic diarrhea or malabsorption. Shortly thereafter, it was determined that bile supplied the gastrointestinal tract with ≈ 227 nmol folate/d (10), and it was hypothesized that bile folate excreted in feces may play a significant role in depleting body folate stores. Other findings that emerged from isotope use include identifying pteroylmonoglutamate metabolites in human urine (11, 12) and elucidating such processes as the need to convert [¹⁴C]pteroylpolyglutamate to [¹⁴C]pteroylmonoglutamate before absorption (13), folate reduction and methylation (14), and liver to blood displacement of folate (15). The biphasic nature by which ¹⁴C from an oral dose of [¹⁴C]pteroylmonoglutamate is eliminated in urine suggested the presence of 2 (folate) analytes, which together accounted for only 10% of the daily folate intake (16).

¹ From the Departments of Nutrition (YL, SRD, JRF, AA, and AJC) and Animal Science (JGF), University of California, Davis; the Cancer Center (PDS) and Pathology Department (JWM and RG), University of California Davis Medical Center, Sacramento; the Center for Accelerator Mass Spectrometry, Lawrence Livermore National Laboratory, Livermore, CA (BAB and JSV); and Integrative Bioinformatics Inc, Rockville, MD (RDP).

² Supported by NIH DK 45939 and Research Resource Grant RR-13461 from the NIH. The study was performed in part under the auspices of the US Department of Energy by the University of California Lawrence Livermore National Laboratory under contract no. W-7405-Eng-48.

³ Reprints not available. Address correspondence to AJ Clifford, Department of Nutrition, University of California, One Shields Avenue, Davis, CA 95616-8669. E-mail: ajclifford@ucdavis.edu.

Received October 9, 2003.

Accepted for publication March 1, 2004.

TABLE 1

Baseline characteristics of and apparent absorption of [¹⁴C]folic acid in the 13 study subjects¹

Subject no. and sex	Age	Body weight	Folate intake	RBC folate	Plasma folate	Plasma vitamin B-12	Plasma homocysteine	[¹⁴ C]Folic acid apparent absorption ²
	<i>y</i>	<i>kg</i>	<i>nmol/d</i>	<i>nmol/L</i>	<i>nmol/L</i>	<i>pmol/L</i>	<i>μmol/L</i>	
1, M	39	111.4	1066	1646	40.7	661	7.9	0.83
2, F	28	52.3	1032	1768	45.4	266	8.5	0.77
3, F	24	56.8	1104	1160	43.9	132	8.6	0.96
4, M	57	90.0	624	1676	25.1	276	8.9	0.89
5, M	30	80.9	710	1793	22.4	280	8.8	0.97
6, M	24	95.5	381	1133	18.3	222	9.7	0.65
7, M	24	84.1	2218	1455	56.6	382	6.8	0.68
8, F	25	102.3	651	1433	30.4	246	8.2	0.67
9, M	23	70.5	907	946	44.6	453	6.7	0.85
10, M	21	109.1	952	1927	35.8	483	7.9	0.65
11, F	34	55.5	1057	1525	28.0	325	5.2	0.80
12, F	34	56.8	766	1961	66.6	364	5.7	0.73
13, F	56	52.3	2120	2075	56.0	303	7.7	0.83
$\bar{x} \pm$ FSD	32 ± 0.38	78.3 ± 0.28	1046 ± 0.52	1577 ± 0.22	39.5 ± 0.37	338 ± 0.40	7.7 ± 0.17	0.79 ± 0.14

¹ Weight, folate intake, and concentrations of the blood variables did not change significantly during the study, so they served as steady state values. RBC, red blood cell; FSD, fractional SD (SD/mean).

² (Dose of ¹⁴C – feces ¹⁴C)/dose of ¹⁴C. Feces ¹⁴C (unabsorbed portion of dose) was determined from the *y* axis intercepts of the regression of the flat portion of the data in the top panel of Figure 1 after the first 3 data points.

A limitation of the previous studies was that all but one (16) were of short duration (7 d), thus the isotopes may not have equilibrated fully in body folate pools that turn over the slowest (6–9, 11–15). Because these pools can become key determinants of folate metabolism late in a study, we used accelerator mass spectrometry (AMS) (17) to follow an oral dose of [¹⁴C]pteroylmonoglutamate in 13 healthy adults for longer periods than in previous studies. We used kinetic modeling (18–21) of the data set to quantify and interpret folate metabolism as it might occur *in vivo*.

SUBJECTS AND METHODS

Tracer synthesis, dose preparation, and diet

The Human Subjects Review Committees of the University of California, Davis, and Lawrence Livermore National Laboratory, Livermore, CA, approved the study. Pteroyl-¹⁴C(U)-glutamic acid ([¹⁴C]-pteroylmonoglutamate) was prepared and characterized (22). The specific activity of the administered [¹⁴C]pteroylmonoglutamate was 1.24 Ci/mol. Each orally administered dose consisted of 0.5 nmol [¹⁴C]pteroylmonoglutamate plus 79.5 nmol pteroylmonoglutamate in 125 mL water. Each dose had 100 nCi radioactivity and gave a lifetime-integrated radiologic effective dose of 11 μSv, or 1.1 mrem.

Thirteen free-living adults were enrolled in the study (Table 1). They completed a Health Habits Food Frequency Questionnaire (23) and provided a predose fasting blood specimen that was analyzed to confirm their general health and to provide baseline values as shown in Table 1 (except for absorption data). The general health and baseline values did not change during the study. The subjects also provided a complete 24-h collection of urine and a collection of feces to serve as baseline values. Each subject was dosed at 0700 just before a light breakfast that consisted of a doughnut and coffee (≈10 g fat and ≈300 kcal). Each dose consisted of 0.5 nmol [¹⁴C]pteroylmonoglutamate plus 79.5

nmol pteroylmonoglutamate in 125 mL water and was administered orally. After dosing, complete collections of urine and feces were made for ≥28 and 14 d, respectively. Up to 47 serial blood samples were collected in the 150 d that followed administration of the dose.

Urine was collected into 3-L urine plastic containers (Fisher Scientific, Houston). Urine produced during the first day after dosing was collected as two 6-h collections followed by one 12-h collection. Thereafter, complete 24-h urine collections were made for each subject. Immediately after collection, the time and mass of each urine collection was recorded, 2 representative aliquots (≈40 mL each) from each collection were stored at –80 °C, and the remainder was discarded. The urinary steady state loss of folate was determined from the slope of the regression of urine loss by time since dose.

Feces were collected in 5-L plastic bags, and the production times and weights of each collection were recorded. A volume of 0.5 mol KOH/L equal to 5 times the feces mass was added. The mix was dispersed by using a Stomacher laboratory blender (Fisher Scientific model 3500; Fisher Scientific, Pittsburgh) for 2 min on the high setting followed by incubation at 80 °C for 2 h. This process of mixing and incubating was repeated twice. A representative aliquot (≈40 mL) of each homogenized sample was transferred to a 50-mL polypropylene tube containing glass beads (≈25 g of 6-mm sized beads; Fisher Scientific), shaken on a Wrist-action Shaker (model 75; Burrell Scientific, Pittsburgh) for 4 h, and stored at room temperature until analyzed. Analysis was usually completed within 2 mo of sample collection. The apparent fractional absorption (1 – unabsorbed fraction) was determined by using the first 3 collections of feces. The metabolic fecal steady state loss of folate was determined from the slope of the regression for all data points after the first collections of feces.

Serial blood samples (≤47 samples, ≤10 mL each) were drawn over the first 150 d after dosing into glass tubes that

contained EDTA. The intensity of sampling was high immediately after dosing (≈ 24 in the first day) to monitor rapidly changing conditions (of ^{14}C) in blood during this period. A 0.5-mL aliquot of whole blood was removed from each draw; packed cell volume (PCV) was determined, and the aliquot was stored at -20°C for whole-blood folate analysis (24, 25). The remainder was centrifuged ($1000 \times g$, 10 min, 23°C) to separate the plasma that was collected and stored at -80°C until analyzed. The leukocyte layer (buffy coat atop sedimented erythrocytes) was removed and discarded. The red blood cells (RBCs) were washed 3 times in buffered saline (150 mmol NaCl + 10 mmol K_2HPO_4 + 0.05 mmol EDTA/L water, pH 7.4). The RBCs were resuspended in buffered saline, and their PCVs were determined. They were then stored at -80°C until analyzed. Folate concentrations in plasma and washed RBC suspensions were measured (24, 25). The folate value for washed RBC suspensions was divided by their PCV and expressed as nmol folate/L RBCs. Plasma vitamin B-12 (kit from ICN Biomedicals Inc, Irvine, CA), plasma homocysteine (26), and folate intake (23) were also measured. Laboratory measurement errors had CVs of $\leq 5\%$.

Radiocarbon and total carbon analysis

The ratios of ^{14}C to total carbon in aliquots of plasma (25 μL), lysed erythrocytes (25 μL), urine (75–180 μL), and homogenized feces (50–75 μL), were measured (27). The baseline ^{14}C measurement for each individual was subtracted from its measured isotope ratio. Excess ^{14}C concentrations were converted to folate equivalents (parent compound and all metabolites) by using the specific activity of the dose, its molecular weight, and the total carbon content of each specimen (28). The CVs of our carbon protocols were $\leq 3\%$.

The results are expressed as pmol or nmol [^{14}C]folate/g tissue carbon inferred from the ^{14}C /total carbon measurements. The nmol [^{14}C]folate (including catabolites) per gram of urine carbon times the grams of total carbon/d in the urine was used to determine [^{14}C]folate losses in urine; similar calculations were made for feces. Feces and urine losses were expressed as a fraction of the administered dose (Figure 1, A and B). Urinary ^{14}C losses were also expressed a fraction of the absorbed dose (Figure 1, C).

Kinetic analysis

The data analysis consisted of organizing current concepts of the behavior of human folate metabolism (1–5, 29, 30) into a model suitable for quantitative hypothesis testing (18, 19) and estimating parameters of interest. Our original model consisted of 4 pools of folate; gastrointestinal tract (lumen), plasma, erythrocyte, and viscera (all other tissues), and it lumped all species of visceral folate into a single kinetic compartment and did not distinguish among synthesis, recycling, and catabolism of visceral pteroylpolyglutamate. Irreversible losses of folate (and its metabolites) from the system were assumed to have occurred directly from plasma to urine and from the gastrointestinal tract to the feces. After a review of the scientific literature on folate metabolism, multiple mechanistic hypotheses concerning the process were formulated and tested individually by applying the same experimental protocol to the model that had been used to collect the experimental data. Next, the model predictions were compared with the observed data to seek a mechanistic model capable of accounting simultaneously for the data sets observed for each of the 13 subjects. Model parameters were optimized by

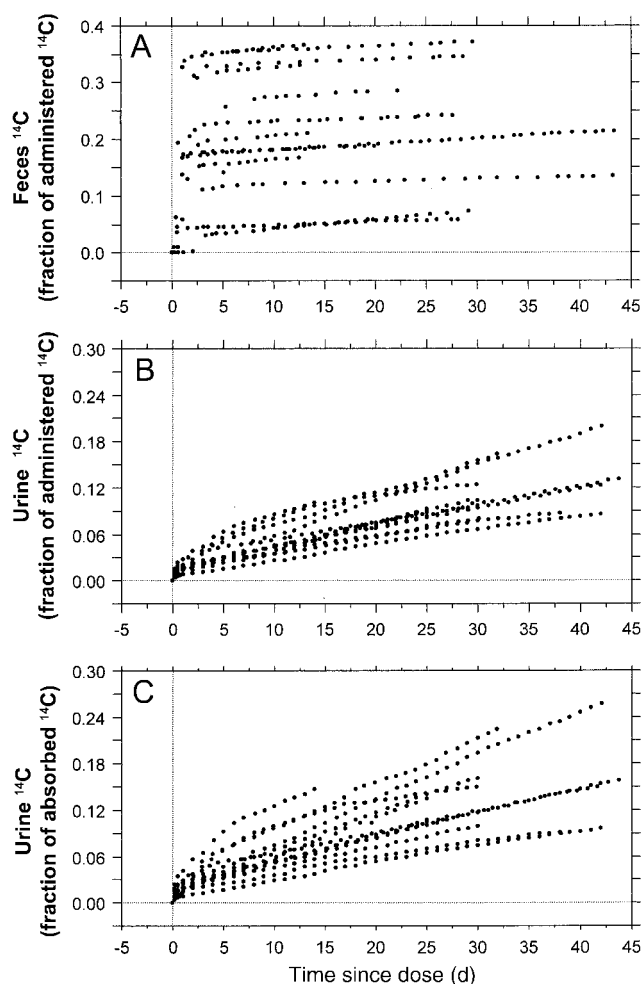


FIGURE 1. Cumulative output of ^{14}C in the feces and urine by the time since dose. The apparent fractional absorption ($1 - \text{unabsorbed fraction}$) was determined by using the first 3 collections of feces. The metabolic fecal steady state loss of folate was determined from the slope of the regression (after the first 3 collections) for each individual subject. The metabolic fecal loss of folate is that which was absorbed and resecreted into the gastrointestinal tract via bile. Each y axis intercept for urine was close to zero, which confirmed the steady state status of each subject. Each slope represents an individual subject's urine loss of folate, mostly in the acetylated form. $n = 13$.

using the SAAM II kinetic analysis software (31, 32), such that hypotheses that were inconsistent with the data sets observed for each of the 13 subjects could be rejected. Some hypothesized processes could not be resolved from the data set, indicating that they either did not occur in vivo or they were transparent to our particular experimental protocol. Finally, if the model is correct, then its parameter, flux, distribution, etc. will usefully inform folate research, but the most important feature of this model is that its quantitative predictions will provide useful tests of its validity.

Single compartments were replaced with true delays, and the actual transit times in Table 2 were extracted from the observed data in Figure 2. Gastric transit time (gastric emptying) is less interesting than is erythron transit time, but it did permit accounting for some of the early plasma data points. The 12 rate constants in Table 3 were estimated (model-estimated) by least-squares fitting of the observed data in Figure 2 to the model in Figure 3. (For individual transit times and rate constants, see Table 1 of

TABLE 2
Steady state delay times¹

Parameter	Delay times (d)		
	Abbreviation	\bar{x}^2	FSD ³
Gastric transit time, to absorption site	delay(1, diet)	0.00293	1.06
Erythron transit time, to circulating ¹⁴ C RBCs	delay(8, 13)	6.15	0.18
Erythrocyte transit time, to RBC demise	delay(5,8)	112	0.09

¹ Estimated directly from least-squares fit of the observed data in Figure 2.

² $n = 13$ subjects.

³ Fractional SD (SD/mean).

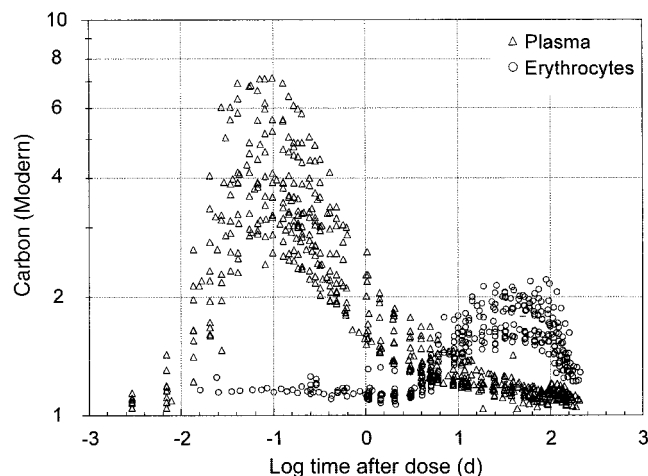


FIGURE 2. Plasma and erythrocyte ¹⁴C radioactivity in subjects 1–13 by time since dose. One Modern = 6.11 fCi (97.94 amol) ¹⁴C/mg total carbon in the specimens. Delays (gastric, erythron, and erythrocyte transit times) were estimated directly from the least-squares fit of the observed data in this figure. The means are presented in Table 2; the delays appear as broken lines in Figure 3.

TABLE 3
Model-estimated steady state daily rate constants (*k*) and fluxes (*f*) of folate¹

Parameter	Abbreviation	Rate constant (d ⁻¹) ²		Analyte flux (nmol/d) ³		
		\bar{x}^4	FSD ⁵	Abbreviation	\bar{x}^4	FSD ⁵
Plasma folate uptake from gastrointestinal tract	<i>k</i> (2,1)	10.39	0.38	<i>f</i> (2,1)	5982	0.98
Marrow folate uptake	<i>k</i> (13,2)	0.29	0.53	<i>f</i> (13,2)	10.1	0.53
Visceral folate uptake	<i>k</i> (5,2)	116.5	0.15	<i>f</i> (5,2)	5897	0.98
Pteroylpolyglutamate synthesis	<i>k</i> (4,5)	0.73	0.42	<i>f</i> (4,5)	1985	0.41
Pteroylpolyglutamate recycling	<i>k</i> (4,5)	0.73	0.42	<i>f</i> (4,5)	1985	0.41
Pteroylpolyglutamate catabolism	<i>k</i> (9,4)	0.0035	0.40	<i>f</i> (9,4)	556	0.43
Urine <i>p</i> -aminobenzoylglutamate loss ⁶	<i>k</i> (0,9)	5.94	0.57	<i>f</i> (0,9)	556	0.43
Urine pteroylmonoglutamate loss	<i>k</i> (0,2)	1.39	0.42	<i>f</i> (0,2)	75	1.23
Folic acid-binding protein folate uptake	<i>k</i> (12,2)	0.092	0.73	<i>f</i> (12,2)	2.6	0.64
Folic acid-binding protein folate release	<i>k</i> (2,12)	0.062	0.47	<i>f</i> (2,12)	2.6	0.64
Folate release into gastrointestinal tract via bile	<i>k</i> (1,5)	1.32	0.36	<i>f</i> (1,5)	5351	1.05
Feces folate loss, includes oxidation products	<i>k</i> (0,1)	0.89	0.70	<i>f</i> (0,1)	415	0.82

¹ See Figure 3 for abbreviations. See Table 1 of Appendix 1 under “Supplemental data” in the current issue at www.ajcn.org for data on individual subjects.

² Donor fraction transferred to recipient compartment.

³ Donor mass transferred to recipient compartment.

⁴ $n = 13$ subjects.

⁵ Fractional SD (SD/mean).

⁶ Mostly as the acetylated form.

Appendix 1 under “Supplemental data” in the current online issue at www.ajcn.org.) If the *k*(0,9) value is allowed to vary, the optimizer chooses to increase its value essentially without limit (in 4 subjects), so we fixed those *k*(0,9) values at 10 (by applying a Bayesian prior; \bar{x} : 5; SD: 3) and concluded that the process was fast but unresolvable because of it being a fast process downstream from a slow process rather because of an inability to partition between *k*(0,9) and *k*(0,2), the precursors of which are kinetically different from each other. The optimizer converged without maximizing the *k*(0,9) value in the remaining 9 subjects; the optimizer-selected value is reported in Table 1 of Appendix 1 under “Supplemental data” in the current online issue at www.ajcn.org. The observed data for subject 4 (a typical subject) appear as symbols along with the corresponding model solutions (fits) as solid lines in Figure 4. Fractional transfers in Table 4 were calculated from the rate constants in Table 3. The residence times in Table 5 were calculated from the rate constants in Table 3. Finally, folate distributions in Table 6 were also model-estimated, and they were supported by the baseline folate intakes in Table 1, which did not change during the study. (See Table 2 of Appendix 1 for individual folate distributions under “Supplemental data” in the current online issue at www.ajcn.org.) A typical SAAM II study file (SAAM II.STU) detailing the model structure and associations between the structure and observed data for a typical (subject 4) is provided in Appendix 2 under “Supplemental data” in the current online issue at www.ajcn.org. The RBC data were fitted to the sum of the RBC compartments and a contribution from plasma trapped between the packed RBCs even after washing. The contribution, quantified as erythrocyte contamination by plasma, P_{contam} , was resolvable for every subject, was <6% on average, and was >10% in only 2 subjects.

Model constraints required that a single model be capable of accounting simultaneously for the following data sets observed for each of the 13 subjects: 1) plasma [¹⁴C]folate, fraction of

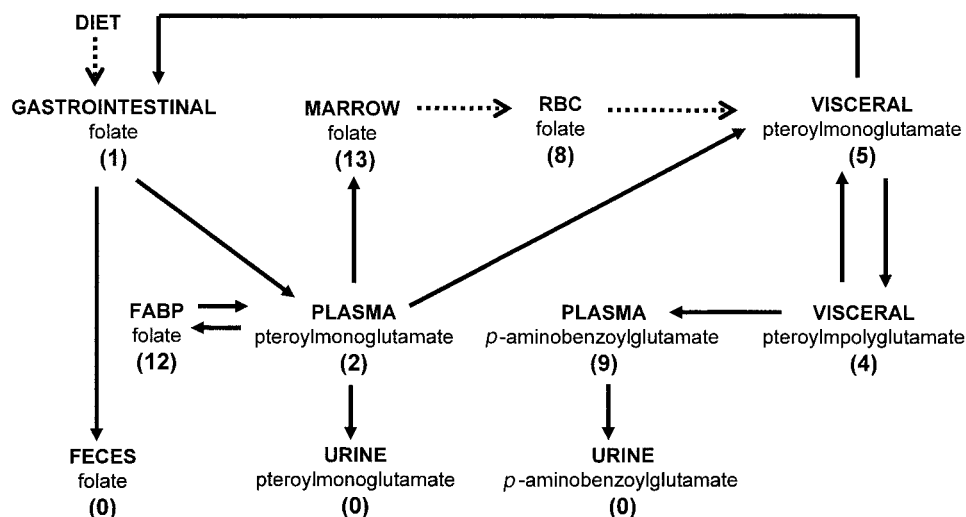


FIGURE 3. Final kinetic model of folate metabolism used to fit the data. The delays referred to in Figure 2 appear as broken lines and were estimated directly from the least-squares fit of the observed data in Figure 2. Rate constants (solid lines), fluxes (solid lines), and distributions (among compartments) were estimated from the model (model-estimated parameters). Feces folate included folate oxidation products, and the urinary *p*-aminobenzoylglutamate was mostly acetylated. The final model included the 12 model-estimated rate constants in Table 3: 4 model-estimated compartments [gastrointestinal tract, marrow, viscera, and folic acid-binding protein (FABP)] and 4 observed compartments [plasma, red blood cells (RBCs), feces, and urine]. The numbers in parentheses are abbreviations for the compartments.

dose/mL; 2) RBC [^{14}C]folate, fraction of dose/mL washed erythrocytes; 3) urinary excretion of ^{14}C , fraction of dose/d; 4) cumulative urinary excretion of ^{14}C , fraction of dose; and 5) cumulative fecal excretion of ^{14}C , fraction of dose. In addition, each

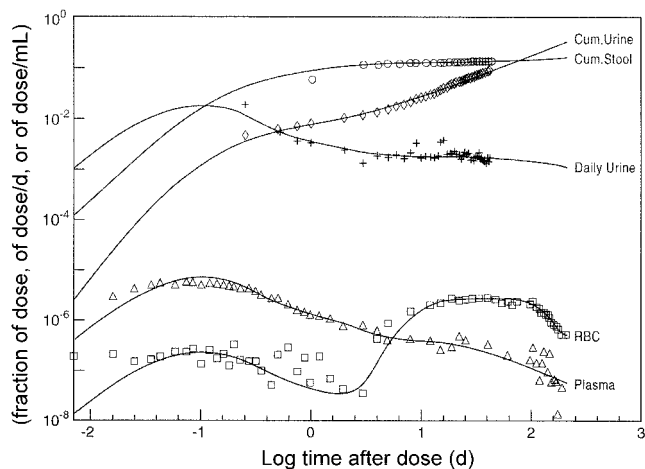


FIGURE 4. Plot of the observed data and model-estimated lines that were fitted to the data from subject 4 with the use of the model in Figure 3. The observed data appear as symbols, and the model solutions appear as solid lines, which are functions of model state variables and parameters that are mapped to the data for direct comparison. The units are a fraction of the dose for cumulative feces and urine, a fraction of the dose/d for daily urine, and a fraction of the dose/mL plasma and red blood cells (RBC). See Appendix 2 (under "Supplemental data" in the current online issue at www.ajcn.org) for a typical SAAM II (SAAM Institute, Seattle) study file detailing the model structure and the associations between model structure and observed data for subject 4 (a typical subject). It was required that a single model account simultaneously for the following data sets collected for each of the 13 subjects: 1) plasma [^{14}C]folate, fraction of dose/mL; 2) RBC [^{14}C]folate, fraction of dose/mL washed erythrocytes; 3) urinary excretion of ^{14}C , fraction of dose/d; 4) cumulative urinary excretion of ^{14}C , fraction of dose; and 5) cumulative fecal excretion of ^{14}C , fraction of dose. In addition, the model was constrained by knowledge of observed steady state measurements for each individual subject. Cum., cumulative.

model was constrained by knowledge of the following observed parameters: 1) steady state concentration of plasma folate, 2) steady state folate content of erythrocytes, and 3) dietary folate intake. Plasma and erythrocyte volumes were estimated as 40 and 25 mL/kg body wt, respectively.

Once a consistent model was developed, each subject was fitted individually to it to obtain subject-specific values for the rate constants, distributions, and delay times. Because the subjects were in steady state with respect to folate metabolism, the ^{14}C tracer data were described by a system of first-order ordinary differential equations with constant coefficients (33). All second-order processes, such as binding and multisubstrate enzymatic reactions, were represented by an effective first-order rate constant, the value for which implicitly incorporates the constant steady state reactant levels. Population means and variances for each parameter were calculated as the mean and variance of the individual's values.

This standard two-stage (STS) calculation was sufficient for our purposes but an iterative two-stage (ITS) parametric population analysis was also performed because it can provide significant increases in statistical power (34). The STS and ITS analyses were performed with the POPKINETICS software package (SAAM Institute, Seattle) in the context of multiple SAAM II files, one for each subject in our study. The main results of our study (Tables 2–6 and Figures 5 and 6) are based on an STS analysis of the individual subjects' kinetic parameters. This is the classic approach for characterizing a population and is based on calculating a simple mean for each model parameter over the group of subjects studied. In the context of population kinetic analysis when the data for each individual subject are sparse, an alternative ITS analysis has the potential to improve population parameter estimates (35, 36), it is computationally attractive (37), and it has been applied to metabolic (20) and pharmacokinetic (21) studies. Several of our subjects were excluded from the PopKin ITS analysis even though, as individuals, they converged successfully. For this reason, we largely

TABLE 4Steady state analyte daily fractional rate constant (*k*) ratios and flux (*f*) ratios calculated from model-estimated data¹

Parameter	Calculation	\bar{x}^2	FSD ³
Rate constant ratios			
Gastrointestinal absorption	$k(2,1)/[k(2,1) + k(0,1)]$	0.92	0.06
Marrow folate uptake from plasma	$k(13,2)/[k(13,2) + k(5,2) + k(0,2) + k(12,2)]$	0.0025	0.56
Urine pteroylmonoglutamate loss from plasma	$k(0,2)/[k(13,2) + k(5,2) + k(0,2) + k(12,2)]$	0.012	0.42
Visceral pteroylmonoglutamate uptake from plasma	$k(5,2)/[k(13,2) + k(5,2) + k(0,2) + k(12,2)]$	0.985	0.005
Intestinal pteroylmonoglutamate uptake (bile) from viscera	$k(1,5)/[k(1,5) + k(4,5)]$	0.65	0.23
Visceral pteroylpolyglutamate synthesis	$k(4,5)/[k(1,5) + k(4,5)]$	0.35	0.43
Visceral pteroylpolyglutamate recycling	$k(5,4)/[k(5,4) + k(9,4)]$	0.70	0.18
Visceral pteroylpolyglutamate catabolism	$k(9,4)/[k(5,4) + k(9,4)]$	0.30	0.42
Flux ratios			
Elimination as pteroylmonoglutamate in feces ⁴	$f(0,1)/[f(0,1) + f(0,2) + f(0,9)]$	0.38	0.45
Elimination as <i>p</i> -aminobenzoylglutamate in urine ⁵	$f(0,9)/[f(0,1) + f(0,2) + f(0,9)]$	0.56	0.32
Elimination as pteroylmonoglutamate in urine	$f(0,2)/[f(0,1) + f(0,2) + f(0,9)]$	0.057	0.63

¹ See Figure 3 and Table 3 for abbreviations. See Table 1 of Appendix 1 under "Supplemental data" in the current issue at www.ajcn.org for data on individual subjects.

² $n = 13$.

³ Fractional SD (SD/mean).

⁴ Includes folate oxidation products.

⁵ Mostly as the acetylated form.

report STS results, even though 3 useful results were gleaned from the ITS analysis. First, the ITS results indicated that 9 of the 16 adjustable parameters were within 20% of the corresponding STS results, thus identifying those parameters that were estimated with small variances for every individual subject. Second, they indicated that 7 of the remaining adjustable parameters were 58–284% of the corresponding STS results, thus identifying individual data sets with less information on the parameter in question and for which the iterative imposition of Bayesian priors will have a greater effect on the outcome. This is potentially of great significance because the extraction of information from fewer data points is cost-effective. Third, the ITS can estimate population variances for each parameter of interest. In our study, for instance, population fractional SDs (FSDs) ranged from 13% to 74%. Because they accurately characterize the variability among individual subjects with respect to various processes of folate metabolism, gathering these population variance estimates should prove valuable when decisions concerning dietary folate requirements of populations are made. A full work sheet containing the model-estimated parameters for each individual subject is available in Tables 1 and 2 of Appendix 1 under "Supplemental data" in the current online issue at www.ajcn.org. A typical SAAM II study file detailing the model structure and the

associations between model structure and observed data is available in Appendix 2 under "Supplemental data" in the current online issue at www.ajcn.org.

RESULTS

The study population consisted of 6 women and 7 men whose observed values (shown in Table 1) suggest a population of healthy adults. Plasma homocysteine ranged from 5.2 to 9.7 $\mu\text{mol/L}$ (\bar{x} : 7.7 $\mu\text{mol/L}$). Intakes and body weights were constant throughout the experiment. Folate intake was correlated positively with plasma folate ($R^2 = 0.3910$, $P = 0.0223$). Plasma folate was correlated negatively with plasma homocysteine ($R^2 = 0.2787$, $P = 0.0637$).

The cumulative output of ¹⁴C in the feces and urine by time since dose is shown in Figure 1, A-C. The unabsorbed fraction of the administered dose (based on the first 3 collections of feces) for individual subjects ranged from 0.03 to 0.35 with a mean of 0.21 (panel A). The apparent fractional absorption (1 – unabsorbed fraction), determined on the basis of the first 3 collections of feces (first 3 data points), ranged from 0.65 to 0.97 (\bar{x} : 0.79); these values did not correlate with intake. Dietary folate absorption (dietary folate \times apparent fractional absorption of folate)

TABLE 5Model-estimated daily residence times¹

Parameter	Calculation, rate constant ratios	\bar{x}^2	FSD ³
Mean residence time as gastrointestinal pteroylmonoglutamate	$1/[k(2,1) + k(0,1)]$	0.100	0.37
Mean residence time as plasma pteroylmonoglutamate	$1/[k(13,2) + k(5,2) + k(0,2) + k(12,2)]$	0.0086	0.15
Mean residence time as plasma <i>p</i> -aminobenzoylglutamate ⁴	$1/k(0,9)$	0.274	0.91
Mean residence time as visceral pteroylmonoglutamate	$1/[k(4,5) + k(1,5)]$	0.525	0.29
Mean residence time as visceral pteroylpolyglutamate	$1/[k(5,4) + k(9,4)]$	119	1.06

¹ See Figure 3 and Table 3 for abbreviations. See Table 1 of Appendix 1 under "Supplemental data" in the current issue at www.ajcn.org for data on individual subjects.

² $n = 13$.

³ Fractional SD (SD/mean).

⁴ Mostly as the acetylated form.

TABLE 6
Model-estimated steady state folate distributions¹

Parameter	Compartment	\bar{x}^2	FSD ³
		nmol	nmol
Gastrointestine	1	591	1.00
Plasma pteroylmonoglutamate	2	51	0.97
Marrow	13	58	0.42
Erythrocyte	8	1111	0.49
Visceral pteroylmonoglutamate	5	4506	1.23
Visceral pteroylpolyglutamate	4	218 338	0.95
Plasma <i>p</i> -aminobenzoylglutamate	9	160	1.47
Plasma folic acid-binding protein	12	52	0.66
Total	—	224 867	0.94

¹ The distributions are supported by the baseline intakes of folate in Table 1 that did not change significantly during the study. See Table 2 of Appendix 1 under “Supplemental data” in the current online issue at www.ajcn.org for data on individual subjects.

² $n = 13$.

³ Fractional SD (SD/mean).

ranged from 248 to 1762 nmol/d (\bar{x} : 826 nmol/d; 1046×0.79); see Table 1. The slope of the regression (for all data points after the first collections of feces) ranged from 0.044 to 0.183, with a mean of 0.105%/d and reflected the steady state metabolic fecal loss of pteroylmonoglutamate and its oxidation products.

The slope of ¹⁴C eliminated in urine by time since dose (all data points) for individual subjects ranged from 0.196% to 0.462%, with a mean of 0.302% of the administered dose/d; the individual *y* axis intercepts ranged from 0.678% to 4.801%, with a mean of 2.055% of the administered dose/d (Figure 1B). The slope of ¹⁴C eliminated in urine by time since dose ranged from 0.207% to 0.679% (\bar{x} : 0.393%) of the absorbed dose/d, and the individual *y* axis intercepts ranged from 0.778% to 5.788% (\bar{x} : 2.635%) of the absorbed dose/d (Figure 1C). The slopes reflected the steady state elimination of folate forms found in urine, such as

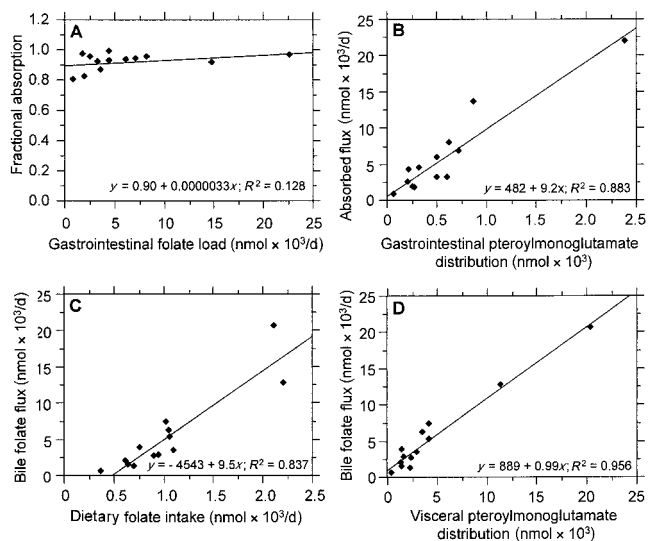


FIGURE 5. Linear relations of steady state model-estimated data in individual subjects (◆). A: Relation of gastrointestinal folate load (diet folate + bile folate) to its fractional absorption [$k(2,1)/(k(2,1) + k(0,1))$]. B: Relation of gastrointestinal pteroylmonoglutamate distribution to its absorbed flux [$f(2,1)$]. C: Relation of dietary folate intake to bile folate flux [$f(1,5)$]. D: Relation of visceral pteroylmonoglutamate distribution to bile folate flux [$f(1,5)$]. See Figure 3 and Table 3 for abbreviations.

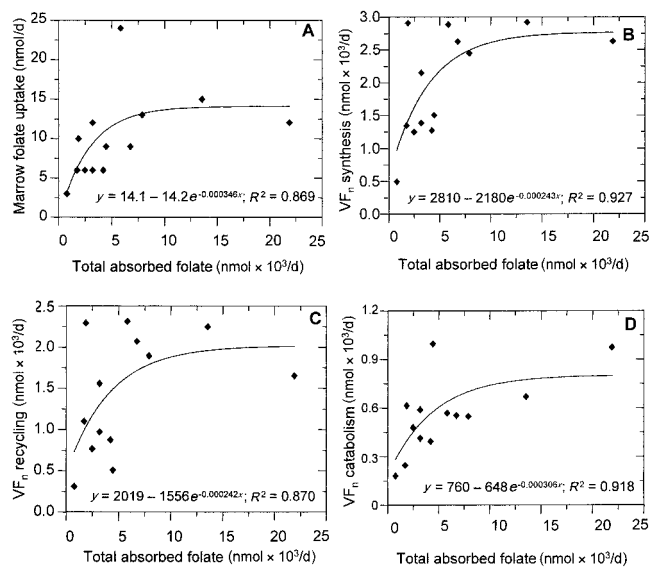


FIGURE 6. Nonlinear relations of steady state model-estimated data to individual subjects (◆). Relation of total absorbed folate [$f(2,1)$] to marrow folate uptake [$f(13,2)$] (A), to visceral pteroylpolyglutamate (VF_n) synthesis [$f(4,5)$] (B), to VF_n recycling [$f(5,4)$] (C), and to VF_n catabolism [$f(9,4)$] (D). See Figure 3 and Table 3 for abbreviations.

[¹⁴C]pteroylmonoglutamate, [¹⁴C]*p*-aminobenzoylglutamate, and [¹⁴C]*p*-acetamidobenzoylglutamate. The *y* axis intercepts were close to zero and indicated that the dose did not perturb steady state folate metabolism in our subjects.

The ¹⁴C values in plasma and erythrocytes by time since dose are shown in Figure 2, where one Modern equals 6.11 fCi ¹⁴C or 97.94 amole ¹⁴C/mg total carbon in these tissues. [¹⁴C]folate first appeared in plasma after a short delay of 0.00293 d and 4.2 min (Table 2), which reflected its transit time through the stomach and duodenum before its appearance in plasma. Peak labeling of plasma occurred at ≈ 2 h and then dropped at a decreasing rate as it entered cells, where it was converted to other forms and sequestered. Finally, the pattern settled into a smooth slow decline toward baseline. The first appearance of ¹⁴C-labeled erythrocytes was delayed by ≈ 6 d, which represented the transit time through the erythron to the appearance of labeled erythrocytes in the circulation. This was followed by a rapid increase in labeled cells that reached a peak at ≈ 20 d and settled into a plateau (≈ 80 d) before declining as aged erythrocytes were removed from the circulation.

The final mechanistic model of folate metabolism that was tested and found to be consistent with the full range of our experimental data is shown in Figure 3. It was used to estimate the parameters described in Tables 3, 5, and 6; to calculate those in Table 4 and in Figures 4 and 5; and to suggest further experimental designs. Compared with the original simple model, the final version of the model had 2 additional compartments (visceral pteroylpolyglutamate and plasma *p*-aminobenzoylglutamate) and 3 additional processes to account for the really informative plasma and urine ¹⁴C kinetics between 4 and 40 d after dosing. The additional processes included visceral pteroylpolyglutamate synthesis (from visceral pteroylmonoglutamate), recycling (to visceral pteroylmonoglutamate), and catabolism (to *p*-aminobenzoylglutamate that went to plasma and eventually to urine as the *p*-acetamidobenzoylglutamate). The catabolic flux of

visceral pteroylpolyglutamate included the flux to visceral pteroylmonoglutamate and the flux to plasma *p*-aminobenzoylglutamate that was eliminated in urine. For visceral pteroylpolyglutamate to serve as a source of plasma pteroylmonoglutamate is not new, but for it to also serve as an immediate precursor to plasma *p*-aminobenzoylglutamate is a new finding.

The added compartments and processes were also assigned physiologically reasonable but tentative identities to facilitate further testing. Finally, the gastrointestinal pool (compartment 1) refers to lumen, but it also must include transepithelial transport, because it delivers absorbed folate to plasma, so it is partly intracellular. Visceral pteroylpolyglutamate refers to intracellular pools.

The observed data and model-fitted plots for a representative subject (subject 4) are shown in Figure 4. Log scaling permitted examination of all the kinetic details on a single plot. Similar results were found for each of the remaining 12 subjects. Observed data appear as symbols, and the corresponding model solutions appear as solid lines. The lines are the functions of model state variables and parameters that are mapped to the experimental data for direct comparison. The cumulative fraction of the dose in stool and urine are shown as are the plasma and daily urine functions that represent contributions from both plasma pteroylmonoglutamate and plasma *p*-aminobenzoylglutamate. Units for the data sets and model curves are fraction of the dose for cumulative feces and cumulative urine, fraction of the dose per day for daily urine, and fraction of the dose per milliliter for plasma and erythrocytes. The lines fit the data from subject 4 extremely well for so complex a system with so many data constraints. The FSDs for the 12 parameter estimates for subject 4 ranged from 0.023 to 0.33. Only plasma and erythrocyte fits had FSDs >0.20.

Although the model accounted for ≈80% of the observed plasma folate concentration for the population (mean of the observed plasma folate/model-estimated plasma folate for each individual subject), it accounted for slightly <40% of the observed erythrocyte folate concentration. Therefore, the fit for the erythrocyte and plasma steady state data were the weakest feature of the model. A combination of underestimated dietary intake and related methodologic issues was the likely cause of the weakness because the rate constants were very well determined by the kinetic data. Normalizing for body weight and folate intake uniformly tightened the plasma FSDs but not those for erythrocytes. So, when a conflict existed between a steady state measurement and the kinetics, we opted for the kinetic data because the rate constants were very well determined from it. Another possible explanation for this lack of agreement lies in the question of how to assign weights to the data. Because the determination of steady state masses is more subject to error than is the determination of tracer abundance, smaller statistical weights were assigned to these data. This means that they had very little effect on the weighted total sum of squares. Consequently, it is possible that assigning far greater statistical weight to the mass data would allow the erythrocyte and plasma steady state data to be fitted more accurately. The decision to weight them lightly was based on the general principle that assigned statistical weights should reflect the certainty with which the numerical data are known. This approach contrasts sharply with other computational approaches, which take measured masses as known with high precision and effectively assign infinite weight to their numerical

values. Experimental realities appear better reflected in the decision to weight these measurements lightly.

The model could not resolve a release of visceral pteroylmonoglutamate to plasma directly because, late in the study, the plasma data were dominated by a folate distribution that turned over very slowly. We tentatively identified that distribution as visceral pteroylpolyglutamate. There are exchanges between plasma and erythrocyte monoglutamate pools, and release of monoglutamate (as methyltetrahydrofolate) from viscera to plasma surely occurs, but they were not resolvable because biliary losses were so rapidly absorbed. Therefore (and surprisingly), the model does not include a viscera monoglutamate to plasma monoglutamate component even though it is well established in previous studies. Finally, folic acid-binding protein was included because it improved the plasma mass fits in some subjects but was poorly resolved in others, so, although included in the model, there was significant uncertainty in its associated parameter values.

Mean steady state delay times that were estimated directly from least-squares fits of observed data are summarized in Table 2. Folate delay from the time of dose to the time of appearance in plasma was only 4.2 min. Folate delay through the erythron to appearance of labeled erythrocytes in the circulation was ≈6 d. Finally, folate delay through circulating erythrocytes to visceral pteroylmonoglutamate was consistent among subjects, as indicated by an FSD of only 0.09.

Model-estimated steady state daily rate constants (*k*) and fluxes are summarized in Table 3. Rate constants ranged from $k = 0.0035 \times \text{d}^{-1}$ for pteroylpolyglutamate catabolism to $k = 116.5 \times \text{d}^{-1}$ for visceral pteroylmonoglutamate uptake from plasma. Fluxes ranged from 2.6 to 5982 nmol/d. Four interesting points emerge from these data. First, the mass of pteroylmonoglutamate absorbed from the gastrointestinal tract was large—5982 nmol/d, or almost 6 times the dietary folate intake of 1046 nmol/d. Second, the mass of pteroylmonoglutamate released into the gastrointestinal tract via bile was also large—5351 nmol/d, or 4.25 times the dietary intake. Third, the loss of pteroylmonoglutamate (and its oxidation products) in feces was substantial—415 nmol/d, or almost 50% of the dietary intake. Fourth, the flux through the visceral pteroylpolyglutamate catabolism pathway to *p*-aminobenzoylglutamate was also substantial (556 nmol/d), which accounted for >50% of the usual dietary intake.

Mean steady state daily fractional transfers are summarized in Table 4. They ranged in size from 0.0025 for marrow folate uptake from plasma [ie, only a quarter of one percent of plasma folate (0.25%) was destined for marrow uptake] to 0.985 for visceral pteroylmonoglutamate uptake from plasma (ie, 98.5% of plasma folate was destined for visceral pteroylmonoglutamate uptake). Approximately two-thirds (65%) of visceral pteroylmonoglutamate was destined for gastrointestinal uptake via bile, whereas the remaining one-third was for visceral pteroylpolyglutamate synthesis. Finally, 30% of visceral pteroylpolyglutamate was destined for catabolism to *p*-aminobenzoylglutamate, which was eliminated in urine (mostly) as *p*-acetamido-benzoylglutamate, whereas the remaining 70% of visceral pteroylpolyglutamate was recycled to visceral pteroylmonoglutamate. Folate elimination occurred via feces (38% as pteroylmonoglutamate and its oxidation products) and urine (56% as *p*-acetamidobenzoylglutamate and 5.7% as intact pteroylmonoglutamate).

Mean steady state residence times are summarized in Table 5. The mean residence time as plasma pteroylmonoglutamate was

very short, only 0.0086 d or ≈ 12 min. The mean residence time as gastrointestinal pteroylmonoglutamate was also relatively short, 0.1 d or ≈ 2.5 h. The mean residence time as visceral pteroylmonoglutamate was ≈ 12.5 h, whereas that as visceral pteroylpolyglutamate was 119 d. Finally, the mean residence time as plasma *p*-aminobenzoylglutamate was ≈ 6 h.

Mean steady state folate distributions are summarized in Table 6. Total-body folate was 224 868 nmol, visceral folate accounted for $\approx 99\%$ of the total [(4506 + 218 339)/224 868], and $\approx 98\%$ of visceral folate was in the pteroylpolyglutamate form (218 339/222 845). As expected, the smallest distributions were in the plasma, marrow, and folic acid-binding protein compartments.

Processes that were linearly related to one another across subjects are summarized in Figure 5, A–D. The fractional absorption of folate from the gastrointestinal tract was high and independent of the gastrointestinal folate load (panel A). The folate mass absorbed each day was directly proportional to the gastrointestinal folate mass (panel B). The mass of visceral pteroylmonoglutamate released into the gastrointestinal tract via bile (bile folate flux) was directly proportional to the dietary folate intake (panel C) and to the visceral pteroylmonoglutamate mass (panel D). There was no evidence for a saturation of the amount folate absorbed from the gastrointestinal tract (panel B) or of the amount of folate released into the gastrointestinal tract via bile each day (panels C and D). Finally, the amount of pteroylpolyglutamate eliminated in urine (as *p*-aminobenzoylglutamate and its acetylated derivatives) was directly proportional to the total amount of pteroylmonoglutamate absorbed, and there was no evidence of saturation of pteroylmonoglutamate elimination in urine (data not shown).

Processes that could be saturated are shown in Figure 6, A–D. Marrow uptake of pteroylmonoglutamate from plasma was saturated at 14.1 nmol/d (panel A). Visceral pteroylpolyglutamate synthesis was saturated at 2810 nmol/d (panel B). Visceral pteroylpolyglutamate recycling to visceral pteroylmonoglutamate was saturated at 2019 nmol/d (panel C). Finally, pteroylpolyglutamate catabolism to *p*-aminobenzoylglutamate was saturated at 760 nmol/d (panel D). The mass of absorbed folate required each day to sustain these processes at half maximum velocity was ≈ 2000 nmol for marrow pteroylmonoglutamate uptake, ≈ 1800 nmol for visceral pteroylpolyglutamate synthesis, ≈ 1800 nmol for visceral pteroylpolyglutamate recycling, and ≈ 1700 nmol for visceral pteroylpolyglutamate catabolism.

DISCUSSION

The observed values in Table 1 and Figures 1 and 2 suggest a population of healthy adults who consumed diets of natural foods that provided sufficient folate. The apparent fractional absorption values matched exactly those of other investigators (6, 16). The patterns of ^{14}C in urine (Figure 1, B and C) had *y* axis intercepts with a mean of 2.1% of the administered dose (panel B) and 2.64% of the absorbed dose (panel C). These results fit well with those of others (6, 8, 16, 38) and with the remarkable avidity with which tissues remove pteroylmonoglutamate from plasma (8). At a 4.2-min gastric transit time, the pattern of [^{14}C]folate in plasma (Figure 2) was expected from other work (1, 6, 8). The 6.15-d erythron transit time was a new observation that fit well with the weeklong maturation of hematopoietic progenitor cells (39). After the 6-d delay through the erythron, the pattern of

[^{14}C]folate-labeled erythrocytes fit well with the erythrocyte kinetics (40). Therefore, our subjects were normal and they yielded a data set that matched the literature values extremely well. The only mismatches were the model-estimated steady state folate distributions (Table 6), which were almost 5-fold larger than values in the literature (41), and bile folate values, which were ≈ 24 -fold larger than values in the literature (10). Finally, the model identified visceral pteroylpolyglutamate to be a direct precursor of *p*-aminobenzoylglutamate as a new pathway.

The slowly turning over compartment that we identified as the visceral pteroylpolyglutamate distribution could have been represented as a loss pathway (instead of a compartment), but 3 key factors led us to conclude that an explicit compartment was warranted. First, the reverse rate constant was almost identifiable from the data in the sense that its FSD was just $>50\%$. Second, elimination of *k*(5, 4) from the model led to systematic deviations between data and model solution for times >150 d. Third, the urinary component that we suggest arises from plasma *p*-aminobenzoylglutamate is very slow, so the precursor for this plasma pool must be slow also. Once the requirement for a slow precursor was established, we had little choice but to include such a compartment in the model, and whereas we cannot be certain that this compartment (pool) is visceral pteroylpolyglutamate, it nevertheless appears to be a novel, reasonable, and testable working hypothesis. Furthermore, although the examination of correlation and covariance matrices may also identify pools to combine or eliminate to improve a model, such examination provided us no hint that our model would be improved by removing compartment 4 or by combining it with compartment 5. Indeed, our original model did not include compartment 4, and the systematic deviations between its predictions and the data were precisely what drove us to consider the visceral pteroylpolyglutamate distribution as a kinetically and physiologically important compartment. So, an experiment not a model is needed to resolve the body pool size mismatch.

The model in Figure 3 indicated several testable predictions. It predicted that 38% of all outgoing folate was eliminated in feces (Table 4), much of it might have represented that which was catabolized to other species during transit through the lower gastrointestinal tract. The model estimated that the mean folate flux to feces was 415 nmol/d (Table 3, and it matched the 454 nmol/d reported previously (42). This flux included a contribution from diet directly (Table 1) and a contribution from diet + bile (Table 3) that was predicted by our model.

The model-estimated fractional absorption [$(k(2,1)/(k(2,1) + k(0,1))$] ranged from 0.82 to 0.98, with a mean of 0.92 (Table 4). This fractional absorption value included dietary folate (the observed apparent fractional absorption of which was 0.79; Table 1) plus visceral pteroylmonoglutamate, which entered the gastrointestinal tract via bile (the model-estimated fractional absorption of the diet + bile mix was 0.92; Table 4). By difference, the fractional reabsorption of visceral pteroylmonoglutamate that entered the gastrointestinal tract via bile ranged from 0.89 to 1.00, with a mean of 0.96: $[k(2,1)/(k(2,1) + k(0,1))] \times [f(1, \text{diet}) + f(1,5)] - [(\text{dose of } ^{14}\text{C} - \text{fecal } ^{14}\text{C}) / \text{dose of } ^{14}\text{C}] \times \text{dietary folate} / f(1,5)$. It can also be calculated that the mass of pteroylmonoglutamate (that originated from visceral pteroylmonoglutamate via bile) that was reabsorbed ranged from 519 to 20 125, with a mean of 5156 nmol/d [fractional reabsorption $\times f(1,5)$], so only 13.8% of the absorbed folate [826/(826 + 5156)] originated directly from the diet. Dietary folate is in predominantly

the pteroylpolyglutamate form (43, 44), which is considered to have only one-half the bioavailability of pteroylmonoglutamate (41). However, spinach folate and pteroylmonoglutamate are interchangeable sources of folate for humans (45), and refried beans and pteroylmonoglutamate are interchangeable sources of folate for rats (46). Therefore, a more quantitative understanding of the contribution of bile to net folate absorption is a fertile area for future research because the apparent fractional absorption value of 0.79 may be an underestimate.

The model predicted an important role for bile in folate metabolism that is testable. Visceral pteroylmonoglutamate that is transported to the gastrointestinal tract via bile can provide a large pool of extracellular pteroylmonoglutamate (≈ 5300 nmol/d) that could blunt the between-meal fluctuations in folate supply to the cells and sustain folate concentrations during periods of folate deprivation. Our model indicated a 24-fold higher flux of visceral pteroylmonoglutamate via bile (5351 nmol/d) than the widely accepted flux of 227 nmol/d (10). Consequently, a deficiency of bile folate reabsorption could help considerably in creating a folate nutritional state that is marginal or deficient (47–54) and a heightened risk of neural tube defects (55).

Model simulation of a sudden drop in the contribution of bile folate (absorption) in subject 4 showed the following to be a testable hypothesis. On the basis of this subject's parameter values, baseline bile folate flux was 1980 nmol/d [1.41, or his $k(1,5)$ value in Table 1 of Appendix 1 under "Supplemental data" in the current online issue at www.ajcn.org] multiplied by 1404 (his visceral pteroylmonoglutamate distribution in Table 2 of Appendix 1 under "Supplemental data" in the current online issue at www.ajcn.org). His baseline fractional absorption was 0.949 [his $k(2,1)/(k(2,1) + k(0,1))$ in Table 1 of Appendix 1 under "Supplemental data" in the current online issue at www.ajcn.org]. A reduction in his baseline fractional absorption to half yielded a bile folate flux that fell to 1645 nmol/d and a visceral pteroylpolyglutamate distribution that fell only 17% after ≈ 3 y at the reduced fractional absorption level. A drop to only 2.6% of his baseline fractional absorption was required to reduce his bile folate to 227 nmol/d (10) after ≈ 3 y in the presence of normal dietary intake. At this level of fractional absorption (2.6% of baseline), his visceral pteroylpolyglutamate distribution fell to 12% of his baseline value in ≈ 3 y. Faster pools, such as plasma, marrow, and RBC, fell more precipitously.


The model predicted that the fractional absorption of folate was high and independent of the gastrointestinal folate load (Figure 5A). It also predicted that the mass of folate absorbed each day from the gastrointestinal tract showed no evidence of saturation (Figure 5B). Because absorbed folate promptly appears in bile (56), it was anticipated that the bile folate flux would correlate with absorbed folate with no evidence of saturation by either folate intake or visceral folate mass, as shown in Figure 5, C and D.

The model predicted that, across subjects, absorbed folate would saturate marrow folate uptake (Figure 6A), synthesis, recycling, and catabolism of visceral pteroylpolyglutamate (Figure 6, B–D). A plateau was reached for these processes despite continued increases in the amount of the total folate absorbed. Furthermore, the mass of absorbed folate required for half maximum values for these processes was ≈ 2000 nmol/d. These data might prove helpful in determining folate requirements for the prevention and treatment of anemia caused by folate deficiency

or in conditions in which there are increased marrow requirements for folate, such as hemolytic anemias. The information is also of interest because the model predicted that steady state folate distributions (Table 6) were almost 5-fold larger than those in the literature (41).

If the folate requirements for specific metabolic functions can be stipulated, it should be possible to determine the minimum intake to sustain these critical functions. This could be particularly significant where folate deficiency or marginal nutrition status is widespread. Simulation of the sudden cessation of dietary intake in a folate-replete person showed some interesting features of the folate system that are testable. This situation is inherently nonlinear and non-steady state because the system is likely to make adaptations to the loss of dietary folate intake. Nonlinear and non-steady state issues aside, and for the sake of simplicity, we assumed that the rate constants do not change. Under these conditions, both the plasma and erythrocyte folate pools decreased by half of their baseline values within 100–130 d, but required another 200 d for erythrocytes and 300 d for plasma to be reduced by half again. Marrow and visceral pteroylmonoglutamate pools declined by a factor of 2–3 in the first 20 d of deprivation, but thereafter were buffered by the slowly turning over and pivotal pteroylpolyglutamate pool. On the basis of our model, the pteroylpolyglutamate distributions were sustained for hundreds of days in the absence of dietary folate. They declined by a factor of 2 only after 300 d with no intake.

Nonlinearities may significantly alter one or more rate constants as total body folate declines, and the literature describes respective decreases in serum and erythrocyte folate of 75% and 18% (57) and of 60% and 15%, (58) in 4-wk depletion studies. Nevertheless, it is clear that if pteroylpolyglutamates turned over as slowly as deduced from these data, then they will significantly buffer declines in all of the other distributions for ≥ 300 d. Conversely, when these reservoirs have themselves been completely depleted, >300 d of a regular diet of folate will probably be required to replete them. A full nonlinear model of folate metabolism that includes all of its regulatory controls and that is capable of accounting for non-steady state responses remains a fertile area for future research.

The model predicted 2 distinct chemical forms in plasma: pteroylmonoglutamate and *p*-aminobenzoylglutamate. For visceral pteroylpolyglutamate to be recycled by conversion to visceral pteroylmonoglutamate was no surprise, but for visceral pteroylpolyglutamate to also be converted directly to *p*-aminobenzoylglutamate was a new pathway that fits nicely with the recent discoveries of pteroylpolyglutamate catabolism (59). The intact pteroylmonoglutamate that was eliminated in urine represented $\approx 6\%$ of ingested folate, a value that compared well with already published values (38, 58, 60). However, the novel and testable hypothesis represented by our model is that fully one-half of excreted folate was derived from visceral pteroylpolyglutamate and appeared in the urine as *p*-aminobenzoylglutamate (and its metabolic successors). 

We thank the reviewers for their perceptive and helpful comments.

AA, YL, and JRF conducted the experiments. SRD prepared the labeled folic acid. RG, JWM, and PDS covered the clinical aspects of the study. BAB and JSV performed the ^{14}C measurements. RDP constructed the model. AJC designed the study, created the data set for modeling, and drafted the manuscript. JGF, RDP, and AJC interpreted the results and revised the paper. RG and JWM reviewed the semifinal draft. The authors had no conflict of interest.

REFERENCES

- Steinberg SE. Mechanisms of folate homeostasis. *Am J Physiol* 1984; 246:G319–24.
- Shane B. Folate metabolism. In: Piciano MF, Stokstad ELR, Gregory JF, eds. Folic acid metabolism in health and disease. Contemporary issues in clinical nutrition. New York: Wiley-Liss, 1990:65–78.
- Stokstad ELR. Historical perspectives on key advances in the biochemistry and physiology of folates. In: Piciano MF, Stokstad ELR, Gregory JF, eds. Folic acid metabolism in health and disease. Contemporary issues in clinical nutrition. New York: Wiley-Liss, 1990:1–21.
- Shane B. Folate chemistry and metabolism. In: Bailey LB, ed. Folate in health and disease. New York: Marcel Dekker, Inc, 1995:1–22.
- Wagner C. Biochemical role of folate in cellular metabolism. In: Bailey LB, ed. Folate in health and disease. New York: Marcel Dekker, Inc, 1995:23–42.
- Anderson B, Belcher EH, Chanarin I, Mollin DL. The urinary and faecal excretion of radioactivity after oral doses of ^3H -folic acid. *Br J Haematol* 1960;6:439–55.
- Sheehy TW, Santini R Jr, Guerra R, Angel R, Plough IC. Tritiated folic acid as a diagnostic aid in folic acid deficiency. *J Lab Clin Med* 1963; 61:650–9.
- Johns DG, Sperti S, Burgen ASV. The metabolism of tritiated folic acid in man. Montreal: McGill University Clinic, 1961:1684–95.
- Baker SJ, Kumar S, Swaminathan SP. Excretion of folic acid in bile. *Lancet* 1965;1:685.
- Herbert V. Excretion of folic acid in bile. *Lancet* 1965;1:913.
- McLean A, Chanarin I. Urinary excretion of 5-methyltetrahydrofolate in man. *Blood* 1966;27:386–8.
- Saleh AM, Pheasant AE, Blair JA, Allan RN, Walters J. Folate metabolism in man: the effect of malignant disease. *Br J Cancer* 1982; 46:346–53.
- Butterworth CE Jr, Baugh CM, Krumdieck C. A study of folate absorption and metabolism in man utilizing carbon-14-labeled polyglutamates synthesized by the solid phase method. *J Clin Invest* 1969;48:1131–42.
- Perry J, Chanarin I. Intestinal absorption of reduced folate compounds in man. *Br J Haematol* 1970;18:329–39.
- Whitehead VM, Cooper BA, Pratt RF. Absorption of folic acid. *Lancet* 1972;1:326.
- Krumdieck CL, Fukushima K, Fukushima T, Shiota T, Butterworth CE Jr. A long-term study of the excretion of folate and pterins in a human subject after ingestion of ^{14}C folic acid, with observations on the effect of diphenylhydantoin administration. *Am J Clin Nutr* 1978;31:88–93.
- Vogel JS, Turteltaub KW, Finkel R, Nelson DE. Accelerator mass spectrometry: isotope quantification at attomole sensitivity. *Anal Chem* 1995;67:A353–9.
- Phair RD. Development of kinetic models in the nonlinear world of molecular cell biology. *Metabolism* 1997;46:1489–95.
- Phair RD, Misteli T. Kinetic modelling approaches to in vivo imaging. *Nat Rev Mol Cell Biol* 2001;2:898–907.
- Vicini P, Cobelli C. The iterative two-stage population approach to IVGTT minimal modeling: improved precision with reduced sampling. Intravenous glucose tolerance test. *Am J Physiol Endocrinol Metab* 2001;280:E179–86.
- DiCenzo R, Forrest A, Slish JC, Cole C, Guillet R. A gentamicin pharmacokinetic population model and once-daily dosing algorithm for neonates. *Pharmacotherapy* 2003;23:585–91.
- Plante LT, Williamson KL, Pastore EJ. Preparation of folic acid specifically labeled with carbon-13 in the benzoyl carbonyl. *Methods Enzymol* 1980;66:533–5.
- Block G, Hartman AM, Dresser CM, Carroll MD, Gannon J, Gardner L. A data-based approach to diet questionnaire design and testing. *Am J Epidemiol* 1986;124:452–69.
- Lin Y, Dueker SR, Jones AD, Clifford AJ. A parallel processing solid phase extraction protocol for the determination of whole blood folate. *Anal Biochem* 2002;301:14–20.
- Dueker SR, Lin Y, Jones AD, et al. Determination of blood folate using acid extraction and internally standardized gas chromatography-mass spectrometry detection. *Anal Biochem* 2000;283:266–75.
- Gilfix BM, Blank DW, Rosenblatt DS. Novel reductant for determination of total plasma homocysteine. *Clin Chem* 1997;43:687–8.
- Vogel JS. Rapid production of graphite without contamination for biomedical AMS. *Radiocarbon* 1992;34:344–50.
- Pella E. Elemental organic analysis. *Am Lab* 1990;22:116–25.
- Suh JR, Herbig AK, Stover PJ. New perspectives on folate catabolism. *Annu Rev Nutr* 2001;21:255–82.
- Koury MJ. Red blood cell production and kinetics. In: Simon TL, Dzik WH, Snyder EL, Stowell CP, Strauss RG, eds. Rossi's principles of transfusion medicine. 3rd ed. New York: Lippincott Williams & Wilkins, 2002:93–100.
- Barrett PH, Bell BM, Cobelli C, et al. SAAM II: simulation, analysis, and modeling software for tracer and pharmacokinetic studies. *Metabolism* 1998;47:484–92.
- Cobelli C, Foster DM. Compartmental models: theory and practice using the SAAM II software system. *Adv Exp Med Biol* 1998;445:79–101.
- Jacquez JA. Compartmental analysis in biology and medicine. In: Arbor A, ed. Compartmental analysis in biology and medicine. 3rd ed. Ann Arbor, MI: BioMedware, 1996.
- Vicini P, Barrett PH, Cobelli C, Foster DM, Schumitzky A. Approaches to population kinetic analysis with application to metabolic studies. *Adv Exp Med Biol* 1998;445:103–13.
- Steimer JL, Mallet A, Golmard JL, Boisvieux JF. Alternative approaches to estimation of population pharmacokinetic parameters: comparison with the nonlinear mixed-effect model. *Drug Metab Rev* 1984;15:265–92.
- Drusano GL, Liu W, Perkins R, et al. Determination of robust ocular pharmacokinetic parameters in serum and vitreous humor of albino rabbits following systemic administration of ciprofloxacin from sparse data sets by using IT2S, a population pharmacokinetic modeling program. *Antimicrob Agents Chemother* 1995;39:1683–7.
- Beal SL, Sheiner LB. Estimating population kinetics. *Crit Rev Biomed Eng* 1982;8:195–22.
- Cooperman JM, Pesci-Bourel A, Luby AL. Urinary excretion of folic acid activity in man. *Clin Chem* 1970;16:375–81.
- Bills ND, Koury MJ, Clifford AJ, Dessypris EN. Ineffective hematopoiesis in folate-deficient mice. *Blood* 1992;79:2273–80.
- London IM, Shemin D, West R, Rittenberg D. Heme synthesis and red blood cell dynamics in normal humans and in subjects with polycythemia vera, sickle-cell anemia, and pernicious anemia. *J Biol Chem* 1949; 179:463–84.
- Institute of Medicine, National Academy of Sciences. Dietary reference intakes for thiamin, riboflavin, niacin, vitamin B6, folate, vitamin B12, pantothenic acid, biotin and choline. Washington, DC: National Academy of Sciences, 1998.
- Herbert V, Drivas G, Manusselis C, Mackler B, Eng J, Schwartz E. Are colon bacteria a major source of cobalamin analogues in human tissues? *Trans Assoc Am Physicians* 1984;97:161–71.
- Hoppner K, Lampi B, Smith DC. Data on folacin activity in foods: availability, applications, and limitations. In: Folic acid: biochemistry and physiology in relation to the human nutrition requirements. Washington, DC: National Academy of Sciences, 1977:69–81.
- Stokstad ELR, Shin YS, Tamura T. Distribution of folate forms in food and folate bioavailability. In: Folic acid: biochemistry and physiology in relation to the human nutrition requirements. Washington, DC: National Academy of Sciences, 1977:56–68.
- Konings EJ, Troost FJ, Castenmiller JJ, Roomans HH, Van Den Brandt PA, Saris WH. Intestinal absorption of different types of folate in healthy subjects with an ileostomy. *Br J Nutr* 2002;88:235–42.
- Muller HG, Facer MR, Bills ND, Clifford AJ. Exchangeability of food folates in a depletion-repletion rat growth bioassay. *J Nutr* 1996;126: 2585–92.
- Steinberg SE, Campbell CL, Hillman RS. Kinetics of the normal folate enterohepatic cycle. *J Clin Invest* 1979;64:83–8.
- Halsted CH, Robles EA, Mezery E. Intestinal malabsorption in folate-deficient alcoholics. *Gastroenterology* 1973;64:526–32.
- Leonard JP, Desager JP, Beckers C, Harvengt C. In vitro binding of various biological substances by two hypocholesterolaemic resins. Cholestyramine and colestipol. *Arzneimittelforschung* 1979;29:979–81.
- Nikkila EA, Miettinen TA, Lanner A. Treatment of hypercholesterolemia with Secholex. A long-term clinical trial and comparison with cholestyramine. *Atherosclerosis* 1976;24:407–19.
- Hernandez-Diaz S, Werler MM, Walker AM, Mitchell AA. Folic acid antagonists during pregnancy and the risk of birth defects. *N Engl J Med* 2000;343:1608–14.
- Kempainen TA, Kosma VM, Janatuinen EK, Julkunen RJ, Pikkarainen PH, Uusitupa MI. Nutritional status of newly diagnosed celiac disease

- patients before and after the institution of a celiac disease diet—association with the grade of mucosal villous atrophy. *Am J Clin Nutr* 1998; 67:482–7.
53. Lim ML. A perspective on tropical sprue. *Curr Gastroenterol* 2001;3: 322–7.
54. Doyle TJ, Bryan RT. Infectious disease morbidity in the US region bordering Mexico, 1990–1998. *J Infect Dis* 2000;182:1503–10.
55. Hendricks KA, Simpson JS, Larsen RD. Neural tube defects along the Texas-Mexico border, 1993–1995. *Am J Epidemiol* 1999;149: 1119–27.
56. Lavoie A, Cooper BA. Rapid transfer of folic acid from blood to bile in man, and its conversion into folate coenzymes and into a pteroyl- glutamate with little biological activity. *Clin Sci Mol Med* 1974;46: 729–41.
57. Herbert V. Experimental nutritional folate deficiency in man. *Trans Assoc Am Physicians* 1962;75:307–20.
58. Sauberlich HE, Kretsch MJ, Skala JH, Johnson HL, Taylor PC. Folate requirement and metabolism in nonpregnant women. *Am J Clin Nutr* 1987;46:1016–28.
59. Suh JR, Oppenheim EW, Girgis S, Stover PJ. Purification and properties of a folate-catabolizing enzyme. *J Biol Chem* 2000;275:35646–55.
60. Kownacki-Brown PA, Wang C, Bailey LB, Toth JP, Gregory JF III. Urinary excretion of deuterium-labeled folate and the metabolite *p*-aminobenzoylglutamate in humans. *J Nutr* 1993;123:1101–8.